Journal of Materials Chemistry A

Accepted Manuscript

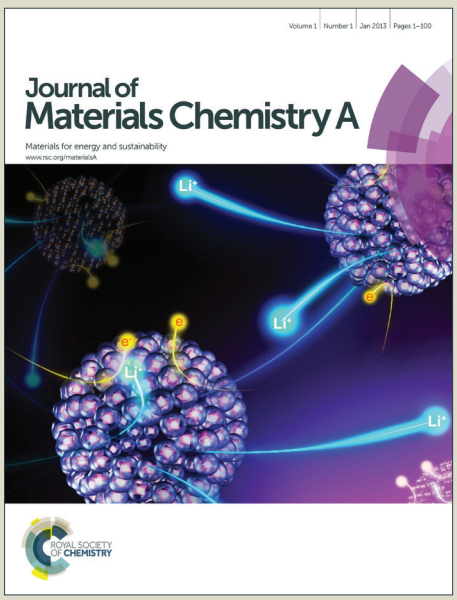

ROYAL SOCIETY OF CHEMISTRY

www.rsc.org/materialsA

Journal Name

RSCPublishing

ARTICLE

Molybdenum Carbide – Carbon Nanocomposites Synthesized from Reactive Template for Electrochemical Hydrogen Evolution

Nawal S. Alhajri, [a] Dalaver H. Anjum, [b] and Kazuhiro Takanabe[a]*

Cite this: DOI: 10.1039/xoxxoooooox

Received ooth January 2012,
Accepted ooth January 2012

DOI: 10.1039/xoxxoooooox

www.rsc.org/

Molybdenum carbide nanocrystals (Mo_2C) with sizes ranging from 3 to 20 nm were synthesized within a carbon matrix starting from a mesoporous graphitic carbon nitride (mpg-C_3N_4) template with confined pores. A molybdenum carbide phase (Mo_2C) with a hexagonal structure was formed using a novel synthetic method involving the reaction of a molybdenum precursor with carbon residue originating from C_3N_4 under nitrogen at various temperatures. The synthesized nanocomposites were characterized using powder X-ray diffraction (XRD), temperature-programmed reaction with mass spectroscopy (MS), CHN elemental analyses, thermogravimetric analyses (TGA), nitrogen sorption, X-ray photoelectron spectroscopy (XPS), and transmission electron microscopy (TEM). The results indicated that the synthesized samples have different surface structures and compositions, which are accordingly expected to exhibit different electrocatalytic activities toward the hydrogen evolution reaction (HER). Electrochemical measurements demonstrated that the sample synthesized at 1323 K exhibited the highest and most stable HER current in acidic media, with an onset potential of −100 mV vs. RHE, among the samples prepared in this study. This result is attributed to the sufficiently small particle size (~8 nm on average) and accordingly high surface area (308 m^2 g^{-1}), with less oxidized surface entrapped within the graphitized carbon matrix.

Introduction

Hydrogen is considered a clean energy carrier and a promising candidate for the replacement of petroleum fuels.[1,2] Currently, most hydrogen for industrial purposes is produced from the steam reforming of natural gas or methane, which generates carbon dioxide as an undesired by-product.[3] The development of alternative technologies for the production of clean energy from renewable resources remains a challenge. The electrolysis of water is achieved by a system associated with a sustainable and greenhouse-gas-free source to generate hydrogen, with the required electricity being derived from renewable energy sources such as sunlight, wind, or geothermal energy.[4-6] During water electrolysis, the hydrogen evolution reaction (HER) occurs, which requires an effective catalyst to reduce the overpotential and consequently increase the efficiency of the reaction. To date, the electrocatalytic HER depends on the use of noble metals, such as Pt, as active and stable electrocatalysts. However, Pt is an expensive metal and suffers from a global supply shortage.[7-14]

Many attempts have been aimed to develop non-noble-metal cathode materials which are required to be active and stable enough to replace the Pt-group metals in extreme conditions. Among them, tremendous attentions are given to d^0 metal sulfides, such as WS^{15} , Mo_2S,[15-17] and metal carbides, such as WC,[18] TaC,[7] and Mo_2C.[19,20] Group VI transition-metal carbides are proved to be stable under a wide range of electrocatalytic operating conditions.[19-22] These compounds exhibit good corrosion resistance, high stability, high melting points, and high mechanical strength.[21]

The experimental and theoretical investigations have been performed to elucidate the electronic structure of metal carbides.[23,24] The hybridization occurs between the metal d-orbitals and the carbon s- and p-orbitals and resulted in an expansion in the d-band structure of the metal, approaching the d-band of Pt.[3,23,24] Thus, group-VI transition-metal carbides possess catalytic properties similar to those of the Pt-group metals, which makes them promising candidates to replace the noble metals in hydrogen-generation catalysts, especially in electrocatalysts.[3,19,20] Antonietti and coworkers,[25-31] and our previous works[7,18,32-34] demonstrated the use of reactive template (mpg-C_3N_4) and urea-glass method to synthesize various metal nitride and carbide nanomaterials. In this method, carbon nitride or urea precursor not only provides confined space for nanoparticle formation, but also chemical sources of nitrogen and carbon. We reported a novel synthetic approach to prepare high-surface-area tantalum nitride/carbide and tungsten carbide utilizing mesoporous graphitic carbon nitride (mpg-C_3N_4) as a reactive template under various conditions.[7,18] The obtained nanomaterials exhibited tremendous improvements in stability and electrocatalytic activity for the HER in acidic media.[7,18] Thus, this synthetic approach to form nanocarbide

crystals presents an opportunity to prepare additional transition-metal carbides and to utilize them in various applications, particularly the electrochemical HER.

It has been known that molybdenum carbides are active in various catalytic reactions, especially carbon conversion and hydrogenolysis-type reactions.[21] As for HER, the electrocatalytic activity of commercial Mo_2C has been investigated and several reports have demonstrated how the use of microparticles would result in low activity.[19,20] Very recently, Chen et al. reported the highly active Mo_2C/carbon nanotube (CNT) composites prepared by relatively simple carburization process. The obtained Mo_2C/CNT exhibited HER cathodic current with an overpotential of 63 mV at 1 mA cm^{-2}, showing the promise of the material as an HER electrocatalyst.[20]

In this study, we designed a novel nanocomposite of molybdenum carbide and carbon via the reaction of a molybdenum precursor with mpg-C_3N_4 at various temperatures under flowing nitrogen. The confinement of mesopores to within a few nanometers was utilized to restrict the size of the molybdenum species, which are surrounded with carbon originating from C_3N_4 decomposition. This system enables direct utilization of the molybdenum species as electrocatalysts. The obtained molybdenum carbide – carbon nanocomposites exhibited a stable and remarkable improvement in their electrocatalytic performance towards HER in acidic media compared with the performance of previously reported bulk materials.

Experimental

Synthesis of mesoporous graphitic carbon nitride

Molybdenum carbide nanocrystals were synthesized via the reaction of a molybdenum precursor with mpg-C_3N_4 as a reactive template. On the basis of a previously published procedure,[25] the template was synthesized by mixing cyanamide (CA, 99%, Aldrich) with an aqueous colloidal silica suspension composed of silica nanoparticles (LUDOX AS-30, 30 wt%, Aldrich) while maintaining a 1:1 weight ratio between SiO_2 and cyanamide. The mixture was heated overnight at 313 K to obtain a solid product. The solid was heated in a semi-closed crucible at 823 K for 4 h. The final product was then thoroughly washed with a 4 M ammonium hydrogen difluoride (NH_4HF_2, ≥98.5% Fluka) aqueous solution to remove the silica, and the product was washed several times with H_2O and ethanol.

Syntheses of molybdenum carbide – carbon nanocomposite

The molybdenum-based nanocomposite was prepared using the reactive hard-templating method. The synthetic procedure was performed while the ratio of mpg-C_3N_4/$MoCl_5$ was maintained at 1:1. First, a dark-green solution was prepared from molybdenum chloride (0.5 g; $MoCl_5$; ≥99.9% Aldrich) dissolved in ethanol (0.5 ml), as described in equation (1):[35]

$$MoCl_5 + 2C_2H_5OH \longrightarrow MoCl_3(OC_2H_5)_2 + 2HCl \quad (1)$$

The pores of the reactive template (0.5 g) were subsequently immersed in the aforementioned solution. The final mixture was placed in an alumina boat crucible and heated to a temperature in the range of 1023 to 1573 K under a 100 ml min^{-1} flow of N_2. At the end of the synthetic procedure, a passivation process was performed by flowing a mixture of 1% O_2 in He at 100 ml min^{-1} at room temperature. Caution is required when using this procedure because the thermal decomposition of C_3N_4 causes the formation of hydrogen cyanide and cyanogen gases.

Characterization

The synthesized samples were characterized using elemental analyses (C, H, and N), X-ray diffraction (XRD), N_2 sorption, thermogravimetric analyses (TGA), X-ray photoelectron spectroscopy (XPS), a temperature-programmed reaction with mass spectroscopy (MS), and transmission electron microscopy (TEM). Elemental analyses were performed using a Flash 2000 Thermo Scientific CHNS/O analyzer. The XRD patterns of the products were collected on a Bruker DMAX 2500 X-ray diffractometer equipped with a Cu Kα radiation source (λ = 0.154 nm). The N_2 sorption studies were conducted using a Micrometrics ASAP 2420 to determine the Brunauer-Emmett-Teller (BET) surface area, the Barrett-Joyner-Halenda (BJH) pore size, and the pore volume. The formation mechanism of molybdenum carbide was investigated by detecting the products in gas phase during nanoparticle synthesis using an OMNI Star (GSD320 O1) portable mass spectrometer equipped with a tungsten filament from Pfeiffer Vacuum. The mass spectrometer was connected at the furnace outlet to study the decomposition products under N_2 flow of 100 ml min^{-1}. Mettler-Toledo TGA/DSC1 Star system was utilized to carry out TGA under a 100 ml min^{-1} flow of air. XPS studies were carried out in a Kratos Axis Ultra DLD spectrometer equipped with a monochromatic Al Kα X-ray source ($h\upsilon$ = 1486.6 eV) operating at 150 W, a multi-channel plate and delay line detector under 1.0 ×10^{-9} Torr vacuum. The survey and high-resolution spectra were collected at fixed analyzer pass energies of 160 and 20 eV, respectively. A transmission electron microscope of model TITAN G^2 80-300 ST was used to characterize the sample morphology and to determine the particle size. The microscope was operated at the electron beam energy of 300 keV. Selected area electron diffraction (SAED) patterns were obtained to determine the inter-planar d-spacings of the crystalline phases present in the samples.

Electrochemical measurements

The electrocatalytic activities of the samples toward the HER were studied using a rotating disk electrode (RDE). The working electrode was first prepared using the following procedure. First, 2 mg of molybdenum-based nanocomposite was dispersed in 169 μL of ethanol and sonicated for 30 min. Then, 56.3 μL of Nafion solution was added to the mixture, and the final solution was sonicated for 30 min. Next, 2 μL of the suspension was drop-coated onto a glassy carbon electrode (GCE) with a geometric surface area of 0.071 cm^2 to provide a weight density of 0.25 mg cm^{-2}. Finally, the electrode was placed in an oven and heated at 373 K under air for 1 h.

The electrocatalytic measurements were conducted using a research-grade potentiostat system (VMP3) from BioLogic Science Instruments. The electrochemical cell used in this study was a three-electrode cell. An Ag/AgCl electrode saturated in KCl was used as a reference electrode. The counter electrode was a carbon rod, and all of the electrodes were immersed in the same electrolyte solution (0.05 M H_2SO_4; Fisher Chemical, trace metal grade). Cyclic voltammetry (CV) experiments were performed at a scan rate of 5 mV s^{-1} from −0.60 to 0.39 V vs. a reversible hydrogen electrode (RHE) for hydrogen evolution while maintaining a constant rotational speed of 1600 rpm. Electrochemical impedance spectroscopy (EIS) was measured

for Mo_2C (commercial) and Mo_2C synthesized at 1323 K in acid solution (0.05 M H_2SO_4) from 1000 kHz to 100 mHz at different HER overpotentials (300, 400 and 500 mV).

Results and discussion

Characterization of the mpg-C_3N_4 template

The XRD pattern (Figure 1A) confirms the graphitic structure of the template. A broad peak was observed at 27.3° which corresponds to the interlayer distance between the g-C_3N_4 sheets with d-spacing of ~0.33 nm.[36] The elemental analysis indicates that the sample has a carbon-to-nitrogen ratio (0.55%) lower than the theoretical value of C_3N_4 (0.75%), which suggests that the carbon nitride sample is nitrogen-rich. This result is attributed to the presence of C-NH_2, 2C-NH, and hydrogen-bonded OH groups or absorbed water molecules on the surface.[18] N_2 sorption experiments were also performed, and the results are presented in Figures 1B and C. According to the International Union of Pure and Applied Chemistry (IUPAC), the acquired graph represents a type-IV isotherm; the isotherm contains a hysteresis loop, which confirms the mesoporous structure of the template (Figure 1B). The BET surface area is 162 m^2 g^{-1}, and the pore volume and average pore size (Figure 1C) are 0.35 cm^3 g^{-1} and 6 nm, respectively.

The mass spectrum in Figure 1D reveals the produced gases during the temperature-programmed decomposition of the mpg-C_3N_4 template under a flow of argon (100 ml min^{-1}) in the temperature range of 318 to 1573 K and at a heating rate of 14 K min^{-1}. The spectrum indicates the formation of hydrogen cyanide (27 amu), nitrogen (28 amu), and cyanogen (52 amu) at approximately 960 K. Further decomposition of C_3N_4 led to the formation of C_3N_x residue which was detected at the outlet of the reactor. At the end of the experiment there were no remaining materials present which confirms a complete volatilization of the template. On the basis of the aforementioned findings, equation 2, which explains the C_3N_4 decomposition at high temperatures under inert condition, can be derived as follows:[18]

$$2C_3N_{(4+x)}H_y \longrightarrow aN_2 + b\mathrm{HCN} + cC_2N_2 + dC_3N_z \quad (2)$$

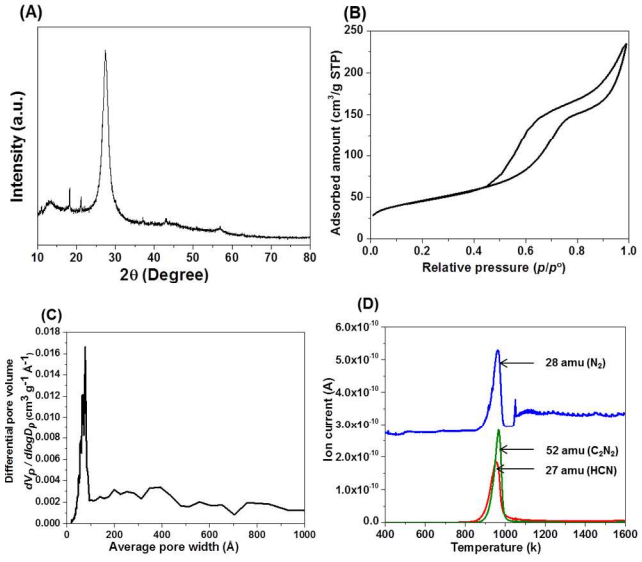

Fig. 1 (A) XRD patterns, (B) N_2 adsorption-desorption isotherms, (C) the pore size distributions obtained from the N_2 desorption studies at 77 K, and (D) MS signals obtained under Ar during the temperature-programmed decomposition of the mpg-C_3N_4 template used in this study.

Temperature-programmed reaction of Mo-C_3N_4 investigated by mass spectroscopy

The reaction pathway of the reactive template C_3N_4 with Mo precursor was investigated by detecting the formed products in gas phase during the syntheses. The MS signals were collected under a flow of inert Ar (100 ml min^{-1}) from 318 to 1573 K at a heating rate of 28 K min^{-1}. The signals for 17, 27, 28, 44, and 52 amu were detected between 600 and 1000 K and were assigned as NH_3, HCN, N_2, CO_2, and C_2N_2, respectively. The spectra of the major four components observed—HCN, N_2, CO_2 and C_2N_2—are shown in Figure 2. The peak maxima were drastically shifted to lower temperatures of approximately 875 K in the case of samples prepared with a molybdenum source, whereas the peak maxima of samples without a molybdenum species were at 965 K. This suggests that a reaction occurred between mpg-C_3N_4 and the molybdenum precursor [$MoCl_3(OC_2H_5)_2$]. The formation of HCN, N_2, and C_2N_2 was consistent with the decomposition product from mpg-C_3N_4; however, the HCN signal was intensified. An increase in the nitrogen signal was also observed, which should indicate the presence of excess carbon as shown in equation 2 (small *z*). As a result, molybdenum-carbon composites are formed, and further temperature increase may lead to molybdenum reacting with the excess carbon. The precursor and remaining solvent likely contained more hydrogen, which improved the formation of the hydrogen-containing gaseous species (HCN and trace NH_3). Likewise, the oxygen-containing product (CO_2), which was detected in the low-temperature region, should originate from the precursor. When equation 2 is unbalanced to release more nitrogen-containing gases, a carbon residue should be formed as a solid; substantial amounts of carbon residue were, in fact, observed, as will be discussed later.

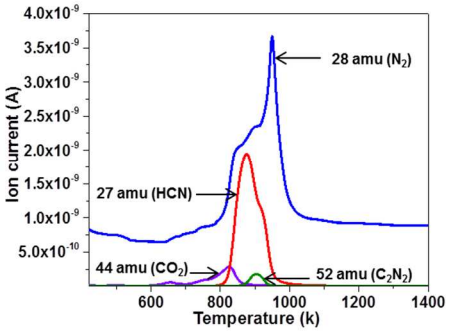

Fig. 2 MS signals obtained during the nanocomposites synthesis under Ar.

X-ray diffraction (XRD)

The produced nanocomposites were characterized by XRD to determine their crystal structure. The XRD patterns are presented in Figure 3 for the samples synthesized under flowing nitrogen at various temperatures from 1023 to 1573 K. The crystallite sizes obtained using the Scherrer equation are listed in Table 1. The XRD pattern for the sample synthesized at 1023

K contains no apparent diffraction peaks, which can be interpreted as the samples consisting of either ultrafine particles or an amorphous phase. In the case of the samples synthesized between 1123 and 1573 K, the XRD patterns contain eight major peaks at 2θ = 34.4, 38, 39,4, 52.2, 61.7, 69.5, 74.5, and 75.3°, which are indexed as (100), (002), (101), (102), (110), (103), (112) planes of hexagonal Mo_2C (PDF-00-001-1188) or (PDF-00-035-0787). This finding confirms that molybdenum carbide was solely formed even at 1123 K, unlike the nitride formation observed in the case of other metals, such as Ti, Nb, and Ta.[7] The peaks become sharper with increasing synthesis temperature, most likely because of the particle aggregation prevalent at high temperatures. The crystallite sizes calculated using the peaks at 52° range from 12 to 52 nm (Table 1). A new shoulder peak appears in the XRD pattern of the sample prepared at 1573 K, consistent with the formation of orthorhombic Mo_2C (PDF-01-071-0242) in addition to the observed hexagonal structure.

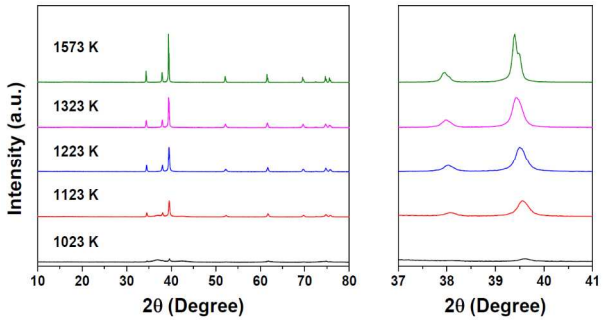

Fig. 3 The effects of reaction temperature on the XRD patterns of molybdenum carbide – carbon nanocomposites synthesized under N_2 flow.

Elemental analyses (CHN)

Elemental analyses were performed to determine the elemental compositions of carbon and nitrogen in the synthesized samples. The results shown in Table 1 indicate that the nitrogen content was very low, even at 1023 K, which confirms that the nitrogen was almost completely gasified at temperatures below 1023 K, as indicated by the MS signals (Figure 2). The carbon content slightly increased from 21% to 24% with increasing reaction temperature. The carbon content exceeded the theoretical stoichiometry in the molybdenum carbide phase Mo_2C (6%), which suggests the presence of excess carbon in a separate phase that is either amorphous or graphitized. This result confirms that molybdenum carbide nanocrystals are present in carbon matrix which accordingly form nanocomposite structure that affects the electrocatalytic activity as will be discussed in the electrochemical measurement section.

Transmission electron microscopy (TEM)

TEM observations were performed on the samples synthesized at temperatures from 1023 to 1573 K. The TEM images and SAED patterns of the samples are presented in Figure 4. The sample synthesized at 1023 K (Figure 4A) contained very fine spherical particles with a size of ~2-5 nm in the matrix of the carbonaceous species, apparently utilizing the confinement effects of such small spacings (Figure 1C). The corresponding SAED pattern reveals three diffraction rings with radii of 0.243, 0.209, and 0.147 nm; these radii correspond to the interatomic spacings of the (002), (102), and (110) planes of the hexagonal Mo_2C crystal structure, respectively. Excess carbon that originated from a residue of the C_3N_4 template was observed between the nanoparticles of the sample. As shown in (Figure 4B), the sample synthesized at 1123 K contains small spherical nanoparticles in the 4-10 nm size range. The SAED pattern reveals three diffraction rings with radii of 0.179, 0.149, and 0.126 nm; these radii correspond to the interatomic spacings of the (102), (110), and (112) planes of the Mo_2C hexagonal crystal structure, respectively. These results are consistent with the XRD patterns presented in Figure 3. The TEM image in Figure 4C (1223 K) shows the formation of small nanoparticles in the 8-15 nm size range. The carbonaceous residue resulting from the low-temperature synthesis is less prominent in this image, which indicates that the reaction of the carbon residue with the Mo precursor was enhanced at higher temperatures. The SAED pattern contained three diffraction rings with radii of 0.256, 0.231, and 0.127 nm; these radii correspond to the (100), (101), and (112) crystal planes, respectively, of the hexagonal Mo_2C structure. In the case of the TEM image of the sample prepared at 1323 K (Figure 4D), the size of the nanoparticles range from 12 to 25 nm. The carbonaceous residue observed at lower temperatures was almost entirely consumed during the formation of carbide nanoparticles at 1323 K. The corresponding SAED pattern revealed additional diffraction rings, which indicated an increase in the particle size and crystallinity of the sample compared with those of the samples synthesized at lower temperatures. The corresponding SAED pattern reveals three strong rings with radii of 0.241, 0.263, and 0.234 nm; these radii correspond to the (002), (100), and (101) crystal planes, respectively, of the hexagonal Mo_2C structure. In addition, a 1 nm crystalline layer with a d-spacing of 0.35 nm was observed around the Mo_2C nanoparticles. The obtained d-spacing corresponds with the interatomic spacings of graphitized carbon.[37] The sample synthesized at 1573 K (Figure 4E) contained nanoparticles in the size range of 15-35 nm, which suggests that the nanoparticles aggregated. The corresponding SAED pattern also revealed additional diffraction rings with radii of 0.260, 0.153, and 0.131 nm; these radii correspond to the interatomic spacings represented by the (100), (110), and (112) planes, respectively, of the hexagonal Mo_2C structure. Similarly, the Mo_2C nanoparticles were surrounded by a thicker layer (2 nm) of graphitized carbon.

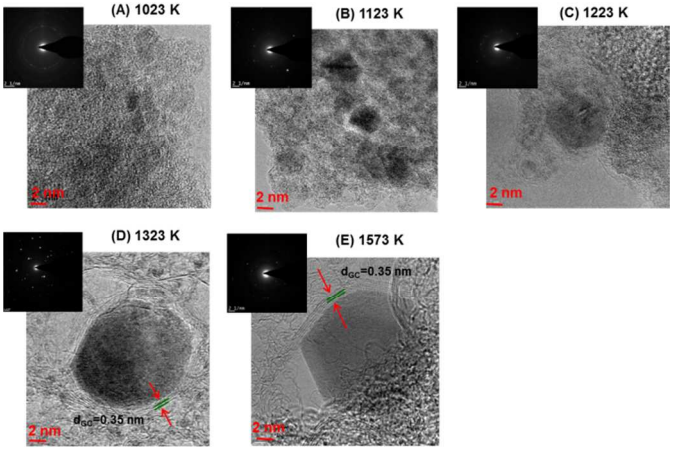

Fig. 4 TEM micrographs of molybdenum carbide – carbon nanocomposites synthesized at different temperatures.

Overall, the TEM images clearly show the successful formation of nanocrystals using the confinement of the mpg-C_3N_4 reactive template. The amount of carbon residue involved in the formation of Mo_2C nanoparticles gradually decreased with increasing temperature until being completely consumed at 1323 K. The produced Mo_2C nanoparticles then combined and aggregated at 1573 K. The size of the nanoparticles at different temperatures exhibits a bimodal distribution. The first distribution begins at a size of ~2 nm at 1023 K, followed by a gradual increase in the size. The number of such produced nanoparticles appeared to increase when the reaction temperature was increased to 1573 K. This result should correlate to the creation of graphitic carbon, which protects the particles from growing. For the second distribution, the obtained nanoparticles at 1023 K are larger than ~5 nm. As the reaction temperature was increased, the size increased to 35 nm at 1573 K because of particle aggregation. Essentially, such aggregation leads to a decrease in the number of active surface sites with increasing reaction temperature. This result suggests that some of the Mo_2C nanoparticles aggregate beyond the confined size of the mpg-C_3N_4 pores. At temperatures greater than 1223 K, the carbon residue clearly graphitized, as observed in the layered structure surrounding the Mo_2C nanoparticles in the TEM images; the thickness of this structure increased with increasing temperature. The graphitized carbon on the surface might affect the electrocatalytic activity of Mo_2C toward the HER.

N_2 sorption

N_2 sorption measurements were performed to determine the BET surface area of the synthesized samples. The results are listed in Table 1, and demonstrate that the surface area of the products increased from 120 to 308 $m^2\ g^{-1}$ with increasing reaction temperature. Apparently, the graphitized carbon residue greatly contributes to the surface area. The obtained high surface area of the produced Mo_2C nanoparticles would significantly enhance the catalytic performance by providing abundant catalytic sites.

According to the MS and TEM results, C_3N_4 decomposed below 1050 K and the remaining carbon originating from the decomposition reacted with the molybdenum precursor to produce Mo_2C nanoparticles. The increase in surface area with increasing reaction temperature resulted from an increase in the production of Mo_2C nanoparticles and porous graphite. The porosity formation was maximized at 1323 K in this case, giving the highest surface area (308 $cm^2\ g^{-1}$). When the reaction temperature was increased further to 1573 K, the produced Mo_2C nanoparticles combined and aggregated, which caused a sudden decrease in the surface area.

Table 1 Synthesis temperature, elemental analyses, phase assignments from the XRD diffractograms, crystallite size evaluations from the Scherrer equation, and BET surface areas for molybdenum carbide – carbon nanocomposites obtained at various temperatures under N_2 flow.

Temperature (K)	C (%)	N (%)	Phase	Crystalline size (nm)	Surface area ($m^2\ g^{-1}$)
1023	21	1.3	Mo_2C	12	120
1123	21	0.9	Mo_2C	26	141
1223	22	0.6	Mo_2C	27	300
1323	22	0.4	Mo_2C	31	308
1573	24	0.0	Mo_2C	52	277

X-ray photoelectron spectroscopy (XPS)

XPS measurements were performed to study the surface chemical compositions and oxidation states of the samples. The Mo 3d, O 1s, and C 1s spectra are presented in Figure 5. The Mo 3d XPS spectra (Figure 5A) of the samples synthesized from 1023 to 1323 K contained two peaks that decreased in intensity with increasing reaction temperature. These peaks were observed at the following binding energies: 235.6 and 232.5 eV for Mo $3d_{3/2}$ and Mo $3d_{5/2}$, which were assigned to Mo^{6+} (MoO_3);[38,39]Additional peak at 228.7 eV for Mo $3d_{5/2}$, was observed in the sample synthesized at 1023 K and was assigned to Mo^{4+} (MoO_2).[40] For the samples synthesized at 1123, 1223, and 1323 K, the Mo $3d_{5/2}$ signal observed at 228.1 eV increased in intensity with increasing reaction temperature.[41] This peak became prominent and shifted to 228.0 eV at 1573 K, which confirms the formation of Mo_2C.[39,41] In addition to this peak, a Mo $3d_{3/2}$ signal was observed at 231.3 eV in the spectrum of the sample prepared at 1573 K; this signal was close to 231.1 eV characteristic value of Mo_2C.[42] The O 1s spectrum (Figure 5B) for samples prepared at temperatures from 1023 to 1323 K contained a characteristic signal at 530.4 that was assigned to O^{2-} in MoO_3; the intensity of this signal decreased with increasing reaction temperature.[39] The C 1s XPS spectra (Figure 5C) contained a characteristic peak attributed to graphite at 284.4 eV.[43] This peak became sharper with increasing reaction temperature, indicating that the concentration of graphitized carbon increased with increasing reaction temperature.

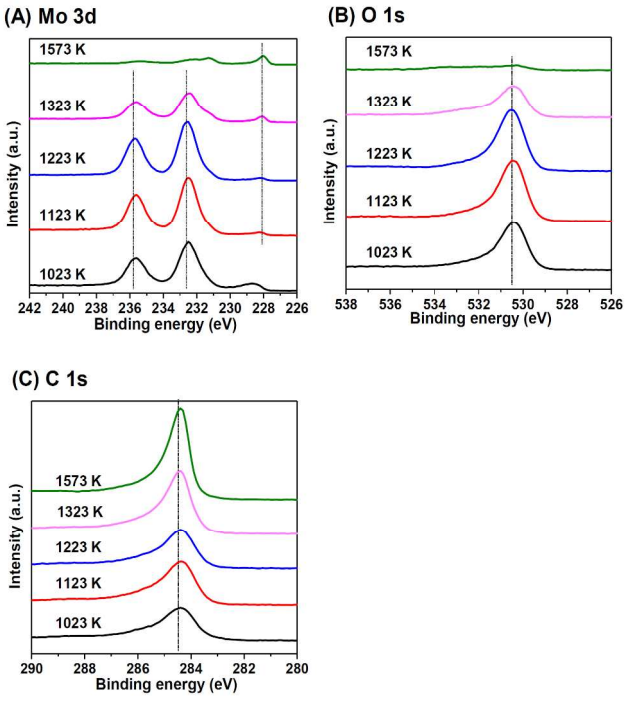

Fig. 5 XPS spectra for (A) Mo 3d (B) O 1s and (C) C 1s of molybdenum carbide – carbon nanocomposites obtained at different temperatures under N_2 flow.

According to the XPS results, an oxide layer formed on all of the samples but decreased in intensity with increasing reaction temperature until almost disappearing at 1573 K. This oxide layer resulted from the passivation process that occurred at the end of the synthetic procedure when the samples were

exposed to ambient air after being removed from the furnace at room temperature. The C 1s XPS spectrum indicates the formation of crystalline layers of graphitized carbon that increased in concentration with increasing reaction temperature. This result is consistent with the elemental analysis, XRD, and TEM results. Thus, not only the carbide species but also the oxide layers on the surface (as an insulator) play a key role in determining the electrocatalytic activities of the materials toward the HER, as will be discussed later.

Thermogravimetric analyses (TGA)

TGA analyses of the synthesized samples under flowing air up to 1273 K were performed to provide an estimate of the composition of the synthesized material and to predict its thermal stability in air. Whereas oxidation of the carbonaceous residue is expected to decrease the weight of the samples, the oxidation of molybdenum carbide species leads to an increase in weight. The TGA results are displayed in Figure 6. For samples synthesized at temperatures less than 1323 K, a slight weight loss below 500 K was detected, which indicates that the samples might adsorb a small amount of water on their surface. However, an obvious weight loss occurred in the temperature range of approximately 620 to 720 K, which was attributed to oxidation of carbonaceous residue from the C_3N_4 remaining in the samples. The decrease in weight continued to 800 K in the case of the sample synthesized at 1023 K, which was due to the presence of a large amount of carbon residue. The samples then oxidized and remained stable until 1050 K. For the samples synthesized at high temperatures, i.e., at 1323 and 1573 K, a small weight loss was observed between 600 and 700 K, which is attributed to the decomposition of a small amount of carbonaceous residue. When the heating exceeded 720 K, the Mo_2C samples began to oxidize to molybdenum trioxide and carbon dioxide (the theoretical increase in percent weight from Mo_2C to MoO_3 is 141%). The weight gain remained almost constant until 1050 K, where a sudden decrease that indicated the complete evaporation of molybdenum trioxide was detected. The TGA results suggest that complex oxidation of the materials occurred for carbon and molybdenum species. At 1323 K, the more extent of carbide phase is proven to exist as observed at weight increase above 800 K.

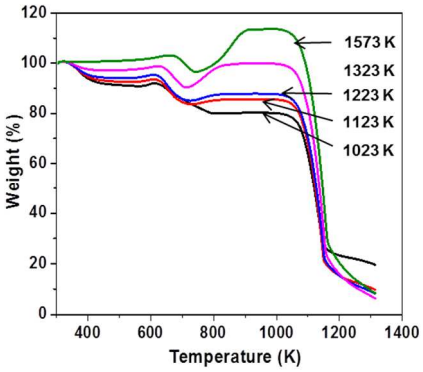

Fig. 6 TGA of molybdenum carbide – carbon nanocomposites synthesized at different temperatures under air flow.

Discussion regarding molybdenum carbide – carbon nanocomposite syntheses

Overall, molybdenum carbide nanoparticles with sizes ranging from 2 to 50 nm that were surrounded with a graphitic carbon matrix were synthesized by the reaction of a C_3N_4 template with a molybdenum precursor under flowing nitrogen at various temperatures from 1023 to 1573 K. The smaller size of the obtained Mo_2C (~2 nm) at 1023 K compared with the pore size of mpg-C_3N_4 (~6 nm) implies that crystal growth occurred before the complete decomposition of the mpg-C_3N_4 framework. The mass spectroscopy results (Figure 2) confirmed the gasification of nitrogen present in the carbon nitride template and that molybdenum carbide formed through the reaction of the molybdenum precursor with the carbon residue originating from the decomposition of C_3N_4. The TEM images (Figure 4) confirm that the size distribution of the nanoparticles produced at various temperatures is bimodal; i.e., 1) only a gradual increase in the size (~2-15 nm) that coincides with an increase in the number of produced nanoparticles was observed, and 2) the nanoparticles extensively aggregated to form particles approximately 50 nm in size. These findings result from the reaction of the molybdenum precursor with the carbon residue originating from C_3N_4 inhibiting or facilitating the aggregation with increasing reaction temperatures (i.e., the carbo-thermal reduction process). The observed increase in the surface area with increasing reaction temperature resulted from the production of graphitized carbon in conjunction with an increase in the number of Mo_2C nanoparticles with increasing temperature as explained in the first model in TEM section. The amount of carbon residue involved in the formation of Mo_2C nanoparticles gradually decreased with increasing reaction temperature until being completely consumed at 1323 K. Then the produced Mo_2C nanoparticles subsequently combined and aggregated when the temperature increased further to 1573 K, which caused a sudden decrease in the surface area. At low temperatures, the unreacted carbonaceous residue captured the Mo_2C nanoparticles and formed aggregates that were connected between the particles. At temperatures above 1223 K, the carbon residue graphitized and formed layers surrounding the Mo_2C nanoparticles, which increased in thickness at 1573 K.

Because of the small size of the produced Mo_2C nanoparticles (~2-15 nm), their surfaces became easily oxidized after they were exposed to ambient air. The XPS results (Figure 5) suggest that the oxide layer decreases with increasing reaction temperature. This result occurs because, at low temperatures, the size of the produced Mo_2C nanoparticles is smaller and they are unstable compared with the particles obtained at high temperatures. At 1573 K, almost no oxide was observed due to the large particle size of Mo_2C, which enhanced its stability and inhibited oxidation.

Molybdenum carbide – carbon nanocomposite as electrocatalysts for the HER

Nanoparticle synthesis is essential to improving HER performance by increasing the number of catalytically active sites. It is known that molybdenum carbide nanoparticles exhibit good electrocatalytic activity toward HER. Our synthesis method of molybdenum carbide nanoparticles not only obtained an increased number of active sites with unique surface facets but also introduced graphitized carbon surrounded Mo_2C nanoparticles which enhanced the conductivity of the nanocomposites and accordingly improved its electrocatalytic activity for HER.

Molybdenum-based nanocomposites synthesized under various temperatures and commercial Mo_2C were tested for the electrochemical HER using an RDE at a constant rotational speed of 1600 rpm. CV experiments were performed in 0.05 M H_2SO_4 at a scan rate of 5 mV s^{-1} between −0.6 and 0.39 V vs.

RHE. The catalytic activity of carbide materials is known to depend on their surface structure and composition. The XPS data (Figure 5) indicates that the surface of the obtained Mo_2C nanoparticles at different temperatures forms MoO_3 layers and that the extent of these oxide layers decreases at high temperatures. Thus, the nanocomposite materials prepared at different temperatures are expected to possess different elecrocatalytic activities.

Figure 7A presents the voltammograms for the molybdenum-based nanocomposites synthesized at various temperatures and commercial Mo_2C. The reported current density was obtained using a geometrical surface area of an electrode (0.07 cm^2) with the same catalyst weight loading (0.25 mg cm^{-2}). The HER cathodic current increased as the reaction temperature was increased from 1023 to 1323 K because of the decreased extent of oxide layers observed on the surface with increasing synthesis temperature. In addition, the surface area increased with increasing reaction temperature, which would increase the number of active sites available on the surface for hydrogen evolution. Molybdenum-based nanocomposites synthesized at 1323 K exhibited the highest HER cathodic current among the samples prepared in this study, with an onset potential of only ~100 mV vs. RHE, similar to the reported values for Mo_2C based materials.[19,20] This highest current density is attributed to the sample's small particle size and accordingly high BET surface area (308 m^2 g^{-1}), which would increase the number of active sites available on the surface for proton adsorption. The presence of 1 nm of graphitized carbon surrounding Mo_2C improved the conductivity and accordingly electron transfer. The extent of oxide layers (as an insulator) observed on the surface of the sample decreased compared with that observed for other samples. Unfortunately, when the reaction temperature was increased to 1573 K, the HER current of Mo_2C decreased and occurred at a relatively higher potential of ~0.15 V vs. RHE because of the sudden decrease in the surface area by particle aggregation. Beneficial effects of nano-sizing are obvious from the result of commercial Mo_2C, particle size of which is large (>100 nm). The stability was tested using Mo_2C synthesized at 1323 K at constant potential of −1.9 V vs. RHE (Figure 7B). The result indicates that the catalytic current decreased to 60% after 3 h and then became stable for 25 h. The slight decrease of HER activity using Mo_2C catalyst is consistent with the literature,[19,20] and the stability of active species remain the issue to be solved.

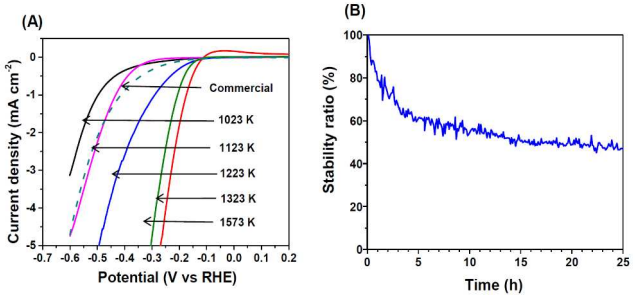

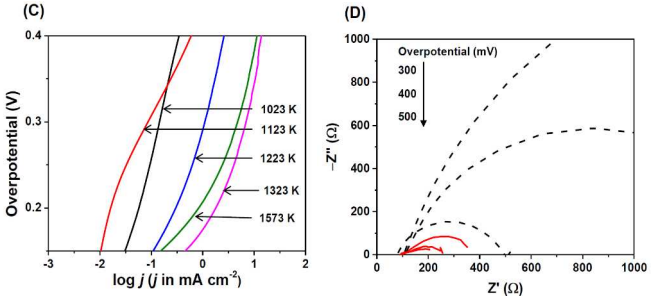

Fig. 7 (A) HER voltammograms of molybdenum carbide – carbon nanocomposites synthesized at different temperatures under N_2 flow and commercial Mo_2C, (B) Stability test of Mo_2C synthesized at 1323 K at –0.19 V vs. RHE, (C) HER Tafel plots for the nanocomposites (0.05 M H_2SO_4 aq., in Ar, 1600 rpm, 5 mV s^{-1}, 298 K), and (D) Nyquist plot of commercial Mo_2C (black dotted lines) and Mo_2C prepared at 1323 K (red solid lines) recorded at different overapotentials (300, 400 and 500 mV) in 0.05 M H_2SO_4.

The differences in electrocatalytic activities were further elucidated between Mo_2C (commercial) and Mo_2C synthesized at 1323 K by electrochemical impedance spectroscopy (EIS) analysis. The result is displayed as Nyquist plot where x- and y-axes are the real and negative imaginary parts of impedance, respectively. The charge transfer resistances for the samples were determined from the semicircle recorded at different overpotentials. Overall, the charge transfer resistances for both samples decreased as the overpotential increased (Figure 7D). The smaller value of impedance for Mo_2C prepared at 1323 K than for commercial Mo_2C is due to the small particle size (~8 nm) that improves minimized distance to the surface. Also, graphitized carbon layer with thickness of about 1 nm around the nanoparticles may function as electronic bridge which will accordingly enhance electronic conductivity and improve electron transfer reaction at the surface of the electrode.

The well-known HER mechanism under acidic solutions includes the following steps:[44]

1. Discharge of a proton to form an adsorbed hydrogen atom (Volmer reaction):

$$M + H_3O^+ + e^- \rightleftharpoons MH_{ads} + H_2O \quad (3)$$

2. Combination of an adsorbed hydrogen atom with a proton and an electron to form molecular hydrogen (Heyrovsky reaction):

$$MH_{ads} + H_3O^+ + e^- \rightleftharpoons H_2 + M + H_2O \quad (4)$$

3. Combination of two adsorbed hydrogen atoms to form molecular hydrogen (Tafel reaction):

$$MH_{ads} + MH_{ads} \rightleftharpoons H_2 + 2M \quad (5)$$

In Eqs. 3-5, M denotes an active site of the catalyst and MH_{ads} denotes a hydrogen atom adsorbed at that site. The HER starts with the proton discharge step (Volmer reaction, Scheme 3) and is followed by either the electrodesorption step (Heyrovsky reaction, Scheme 4) or the proton recombination step (Tafel reaction, Scheme 5).[44]

The HER mechanism can be studied through analysis of the Tafel plots obtained from polarization curves. The Tafel slope (β) is an inherent property of a catalyst and is determined by the

rate-limiting step of the HER. The empirical values of the Tafel slopes extracted from the Tafel plot can provide insight into the probable mechanisms for the HER on the catalytic surface. In acidic solutions, if the Volmer reaction (3) is the rate-determining step or if the rates of (3) and (4) are comparable, a high slope value at room temperature is obtained (≈ 120 mV dec^{-1}). In contrast, a Volmer-Heyrovsky mechanism (4) will return a slope of approximately 40 mV dec^{-1}.[45,46] The Tafel slope of approximately 30 mV dec^{-1}, is known to involve the Volmer-Tafel reaction.[13,44] Tafel slopes (Figure 7C) obtained from the polarization curves from 0.2 to 0.25 V of the molybdenum-based nanocomposites were in the range of 110-235 mV dec^{-1}. These high Tafel slopes are consistent with the Volmer reaction (3) being the rate-determining step and suggest that the surface coverage of the hydrogen species is low and that hydrogen is relatively weakly adsorbed with steady-state kinetics.[13,44]

Conclusions

Molybdenum carbide – carbon nanocomposites were successfully prepared through the reaction of molybdenum precursor with the carbon residue originating from C_3N_4 decomposition under nitrogen at various temperatures. The obtained nanocomposites show that the samples have different surface structures and compositions and are accordingly expected to exhibit different electrocatalytic activities toward the HER. Electrochemical measurements demonstrated that the sample synthesized at 1323 K exhibited the highest and most stable HER current in acidic media among the samples prepared in this study. This result is attributed to the combination of the sample's small particle size (~8 nm on average) and its accordingly high surface area, which was confirmed by BET analysis (308 m^2 g^{-1}), as well as to the graphitized carbon layer on its surface. When the reaction temperature was further increased to 1573 K, the HER current decreased due to particle aggregation, which consequently reduced the surface area of the exposed active sites for hydrogen adsorption. This study clearly demonstrates that the molybdenum carbide-carbon nanocomposites serve as excellent electrocatalysts for the HER, even in highly acidic media. The electrocatalytic performance would be further improved through removing the oxide layers from the surface, enhancement of the dispersion of the nanocrystals in carbon matrix and via the introduction of hetero-atoms.

Acknowledgements

The authors thank Dr. Mohamed Nejib Hedhili at Advanced Nanofabrication, Imaging and Characterization Core Lab, King Abdullah University of Science and Technology for XPS measurements. N.S.A. acknowledges Saudi Aramco for financial support.

Notes and references

[a] *Division of Physical Sciences and Engineering, KAUST Catalysis Center (KCC), King Abdullah University of Science and Technology (KAUST), 4700 KAUST, Thuwal, 23955-6900 Saudi Arabia.*

[b] *Advanced Nanofabrication, Imaging and Characterization Core Lab, King Abdullah University of Science and Technology (KAUST), 4700 KAUST, Thuwal, 23955-6900 Saudi Arabia.*

1 E. Navarro-Flores, Z. Chong and S. Omanovic, *J. Mol. Catal. A,* 2005, **226**, 179.
2 M. S. Dresselhaus and I. L. Thomas, *Nature*, 2001, **414**, 332.
3 W.-F .Chen, J. T. Muckerman and E. Fujita, *Chem.Commun*., 2013, **49**, 8896.
4 W. Kreater, H. Hofmann, *Int. J. Hydrogen Energy,* 1998, **23**, 661. 3.
5 J. A. Turner, *Science,* 2004, **305**, 972.
6 N. S. Lewis and D. Nocera, *PNAS,* 2006, **103**, 15729.
7 N.S. Alhajri, H Yoshida, D.A. Anjum, A.T. Garcia-Esparza, J Kubota, K. Domen and K .Takanabe, *J. Mater. Chem. A*, 2013, **1**, 12606.
8 S. Trasatti, *J. Electroanal. Chem.,* 1972, **39**, 163.
9 J. Greeley, T. F. Jaramillo, J. Bonde, I. Chorkendorff and J. K. Nørskov, *Nature Mater.,* 2006, **5**, 909.
10 E. Santos and W. Schmickler, *ChemPhysChem*, 2006, **7**, 2282.
11 E. Santos and W. Schmickler, *Chem. Phys.,* 2007, **332**, 39.
12 J. K. Nørskov, T. Bligaard, J. Rossmeisl and C. H. Christensen, *Nature Chem.,* 2009, **1**, 37.
13 R. Subbaraman, D. Tripkovic, D. Strmcnik, K.-C. Chang, M. Uchimura, A. P. Paulikas, V. Stamenkovic and N. M. Markovic, *Science,* 2011, **334**, 1256.
14 R. Subbaraman, D. Tripkovic, K.-C. Chang, D. Strmcnik, A. P. Paulikas, P. Hirunsit, M. Chan, J. Greeley, V. Stamenkovic and N. M. Markovic, *Nature Mater*., 2012, **11**, 550.
15 T. Y. Chen, Y. H. Chang, C. L. Hsu, K. H. Wei, C. Y. Chiang, and L. J. Li, *Int. J. Hydrogen Energy*, 2013, **28**, 12302.
16 T. F. Jaramillo, K. P. Jørgensen, J. Bonde, J. H. Nielsen, S. Horch and I. Chorkendorff, *Science*, 2007, **317**, 100.
17 M. A. Lukowski, A. S. Daniel, F. Meng, A. Forticaux, L. Li and S. Jin, *J. Am. Chem. Soc*., 2013, **135**, 10274.
18 A. T. Garcia-Esparza, D. Cha, Y. Ou, J. Kubota, K. Domen, K. Takanabe, *ChemSusChem,* 2013, **6**, 168.21.
19 L. Liao, S. Wang, J. Xiao, X. Bian, Y. Zhang, M. D. Scanlon, X. Hu, Y. Tang, B. Liu and H. H. Girault, *Energy Environ. Sci*, 2014, **7**, 387.
20 W.-F. Chen, C.-H Wang, K. Sasaki, N. Marinkovic, W. Xu, J. T. Muckerman, Y. Zhu, R. R. Adzic, *Energy Environ. Sci.,* 2013, **6**, 943.
21 L. Johansson, *Surf. Sci. Rep.,* 1995, **21**, 177.
22 Y. Liu, T. G. Kelly, J. G. Chen and W. E. Mustain, *ACS Catal*., 2013, **3**, 1184.
23 J. R. Kitchin, J. K. Nørskov, M. A. Barteau and J. G. G. Chen, *Catal. Today*, 2005, **105**, 66.
24 J. G. Chen*, Chem. Rev*., 1996, **96**, 1477.
25 A. Fischer, M. Antonietti and A. Thomas, *Adv. Mater.*, 2007, **19**, 264.
26 A. Fischer, J. O. Müller, M. Antonietti and A. Thomas, *ACS Nano*, 2008, **2**, 2489.
27 A. Thomas, F. Goettmann and M. Antonietti, *Chem. Mater.*, 2008, **20**, 738.
28 Y.-S. Jun, W. H. Hong, M. Antonietti and A. Thomas, *Adv. Mater.*, 2009, **21**, 4270.
29 C. Giordano, C. Erpen, W.-T. Yao and M. Antonietti, *Nano Lett.*, 2008, **12**, 4659.
30 C. Giordano, C. Erpen, W.-T. Yao, B. Milke and M. Antonietti, *Chem. Mater.*, 2009, **21**, 5136.
31 C. Giordano and M. Antonietti, *Nano Today*, 2011, **6**, 366.
32 R. Ohnishi, K. Takanabe, M. Katayama, J. Kubota and K. Domen, *J. Phys. Chem. C,* 2013, **117**, 496.
33 Y. Fukasawa, K. Takanabe, A. Shimojima, M. Antonietti, K. Domen, T. Okubo, *Chem. Asian J*. 2011, **6**, 103.

34 L. Yuliati, J.-H. Yang, X. Wang, K. Maeda, T. Takata, M. Antonietti, K. Domen, *J. Mater. Chem*. 2010, **20**, 4295.
35 G. Raj, *Adv. Inorg. Chem.*, Vol. II, 12th Ed, 2010, Krishna Prakashan Media Ltd., India.
36 M. Groenewolt and M. Antonietti, *Adv. Mater*., 2005, **17**, 1789.
37 R. Wang, J. Yang, K. Shi, B. Wang, L. Wang, G. Tian, B. Bateer, C. Tian, P. Shen and H. Fu, *RSC Adv*., 2013, **3**, 4771.
38 C. Diaz, V. Lavayen and C. Dwyer, *J. Solid State Chem.*, 2010, **183**, 1595.
39 W. Lisowski, A. H. J. van den Berg, L. J. Hanekamp and A. van Silfhout, *Surf. Interface Anal*., 1992, **19**, 93.
40 F. Werfeli and E. Minni, *J. Phys. Chem. Solid State Phys*..1983, **16,** 6091.
41 T. Clair, S. Oyama, D. Cox, S. Otani, Y. Ishizawa, R. Lo, K. Fukui and Y. Iwasawa, *Surf. Sci.*,1999, **426**, 187.
42 E. G. Derouane, V. Parmon, F. Lemos, F. Ribeiro (Sustainable strategies for the upgrading of natural gas, fundamental challenges and opportunities), July, 2003.
43 W. Chen , H. Xu, L. Liu , X. Gao , D. Qi ,G. Peng, S. Tan, Y. Feng, K. Loh, A. Wee, *Surf. Sci.*, 2005, **596**, 176.
44 B. E. Conway and B. V. Tilak, *Electrochim. Acta*, 2002, **47**, 3571.
45 J. G. N. Thomas, *Trans. Faraday Soc*., 1961, **57**, 1603.
46 J. Bockris, I. A. Ammar and K. M. S. Hug, *J. Phys. Chem*., 1957, **61**, 879.

Table of Contents/Abstract Graphic

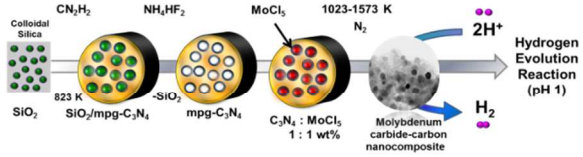

Active Mo_2C-C nanocomposites were synthesized using mpg-C_3N_4 template and demonstrated as an active electrochemical hydrogen evolution.